Commun. Theor. Phys. **76** (2024) 105201 (14pp) https://doi.org/10.1088/1572-9494/ad5272

Flavor mixing and solution structures in Dyson–Schwinger equations for a two-flavor system

Xue-ao Chao[1] **and Yu-xin Liu**[1,2,3,*]

[1] Department of Physics and State Key Laboratory of Nuclear Physics and Technology, Peking University, Beijing 100871, China
[2] Collaborative Innovation Center of Quantum Matter, Beijing 100871, China
[3] Center for High Energy Physics, Peking University, Beijing 100871, China

E-mail: chaoxueao@gmail.com and yxliu@pku.edu.cn

Received 29 May 2024, revised 31 May 2024
Accepted for publication 31 May 2024
Published 31 July 2024

Abstract

We solved the Dyson–Schwinger (DS) equations for a two-flavor system with symmetry to study its flavor mixing effects. Initially, we employed the point interaction model and bare vertex approximation to reveal the structure of the solutions. Using the point interaction model, the DS equations can be solved analytically, and we found that these solutions can be classified into three groups, each forming an ellipse. These solutions exhibit SO(2) symmetry, while the original SU(2) symmetry at the Lagrangian level is dynamically broken to SO(2), corresponding to the emergence of flavor mixing effects. However, this flavor mixing effect does not manifest in the final physical state. By utilizing the system's SO(2) symmetry, we can diagonalize the propagators of the DS equations, eliminating the flavor mixing effect but causing the originally degenerate masses at the Lagrangian level to split. These mass eigenstates have identical quantum numbers but different masses. If we can correspond these to quark particles of different generations, we can explain why the three generations of quarks have different masses and obtain the corresponding quark mass spectrum. Finally, we provide the corresponding numerical results using a more realistic interaction model.

Keywords: Dyson–Schwinger equation, flavor change, mass splitting, dynamic symmetry breaking

(Some figures may appear in colour only in the online journal)

1. Introduction

The standard model (SM) has achieved significant success; however, it fails to explain phenomena, such as dark matter, dark energy, and neutrino masses. Additionally, within SM, unresolved issues, such as the fine-tuning problem, hierarchy problem, mass splitting, and flavor-related questions, persist.

Focusing on flavor issues, three main concerns arise, emphasizing their importance, as 12 of 19 SM parameters are flavor related [1]: (a) Replication: Why are there three generations of fermions, each identical except for mass, and what is their necessity? (b) Fermion mass hierarchy: The significant mass differences between generations are puzzling. For example, the tau lepton is 3600 times heavier than the electron, and the top quark is nearly 100,000 times heavier than the up quark. Neutrinos also seem to exhibit a hierarchical mass structure [2–4]. (c) Mixing hierarchy: The Cabibbo–Kobayashi–Maskawa (CKM) matrix elements exhibit a hierarchical structure.

This study mainly addresses the first two issues, particularly the mass splitting among three generations of quarks. We observed both horizontal and vertical hierarchies in fermion masses, such as $m_u/m_c \sim m_c/m_t \sim \lambda^4$ and $m_d/m_s \sim m_s/m_b \sim \lambda^2$, with $\lambda \approx 0.22$. Quarks, charged leptons, and neutrinos showed mass hierarchies vertically. For instance, first-generation fermions have masses, such as $m_u \sim m_d \sim 5$ MeV

* Author to whom any correspondence should be addressed.

and $m_e \sim 0.5\,\mathrm{MeV}$, with significantly smaller neutrino masses [5].

We observed that quarks participate in strong, electromagnetic, and weak interactions, exhibiting the strongest interactions. Electrons engage in electromagnetic and weak interactions with intermediate strength, whereas electron neutrinos participate only in weak interactions, the weakest of all. The hierarchical structure of interaction strengths, combined with their mass hierarchy, suggests a dynamic origin for their masses. This implies that the Higgs mechanism may itself be dynamic, and the Higgs boson could be composite (see, e.g. [6–9]). This study explored the dynamic origin of mass.

As mentioned earlier, the three generations of fermions with the same charge are identical if there are no mass differences. The fact that mass does not affect the interaction type suggests that they can be treated as the same particles at the interaction level and can replace each other in interactions. This implies a possible symmetry among the three generations, known as horizontal symmetry [1, 10]. Different generations acquire different masses during symmetry breaking. An up quark can potentially transform into other up-type quarks, such as a charm quark, which is dynamically feasible; however, such a transformation is kinematically forbidden due to the conservation of quantum numbers. Therefore, flavor change processes cannot appear as external legs in Feynman diagrams, and the corresponding particles cannot be considered stable particles [11]. Nonetheless, flavor change progress still possibly has multifaceted impacts on many issues, such as CKM and mass splitting. Progress in flavor change and its renormalization have been extensively discussed (see, e.g. [11–13]).

The Dyson–Schwinger (DS) equation is a crucial tool for studying dynamic symmetry breaking [14]. We present a model in which an SU(2) horizontal symmetry dynamically breaks to SO(2). Using the DS equation, there can be a dynamic flavor change progress that generates different masses for different generations.

The remainder of this paper is structured as follows: section 2 describes the theoretical framework. Section 3 discusses the solution structure and numerical results and obtains the mass spectrum for different generation quarks. Section 4 provides a summary of this study.

2. Theoretical framework

2.1. Lagrangian and symmetry

We begin by defining two types of hyperquarks: up-and down-type hyperquarks:

$$\begin{aligned} &\text{up type:} \quad (u_1 \quad u_2),\\ &\text{down type:} \, (d_1 \quad d_2). \end{aligned} \tag{1}$$

Initially, we consider only QCD; the Lagrangian density is given as

$$\begin{aligned} L_0 = {} & \bar{u}_1(i\partial\!\!\!/ - m_{u_1})u_1 + \bar{u}_2(i\partial\!\!\!/ - m_{u_2})u_2 \\ & + \bar{d}_1(i\partial\!\!\!/ - m_{d_1})d_1 + \bar{d}_2(i\partial\!\!\!/ - m_{d_2})d_2 + L_{\mathrm{gluon}}, \end{aligned} \tag{2}$$

where L_{gluon} contains the remaining terms related to gluons. We focus on the up sector first. Because of the simultaneous unified solving of the two flavor systems, the flavor mixing effect must be included. To study the effects of flavor mixing, we must adopt a methodological framework that can describe flavor mixing coherently. The action of one of the families mentioned previously, after renormalization, reads:

$$\begin{aligned} S = \int \mathrm{d}^4x \Big[& Z_2^{11}\bar{u}_1(i\partial\!\!\!/ - Z_m^{11}m_{11})u_1 \\ & + Z_2^{22}\bar{u}_2(i\partial\!\!\!/ - Z_m^{22}m_{22})u_2 \\ & + Z_1 g\bar{u}_1\gamma^\mu A_\mu^a T_a u_1 \\ & + Z_1 g\bar{u}_2\gamma^\mu A_\mu^a T_a u_2 \\ & - Z_3\frac{1}{4}F_{\mu\nu}F^{\mu\nu} - \frac{Z_3}{2\xi}(\partial_\mu A_a^\mu)^2 \\ & + Z_\lambda^{12}\bar{u}_1\lambda_{12}(i\partial\!\!\!/ - Z_m^{12}m_{12})u_2 \\ & + Z_\lambda^{21}\bar{u}_2\lambda_{21}(i\partial\!\!\!/ - Z_m^{21}m_{21})u_1 \\ & + \frac{Z_\lambda^{12}Z_1}{Z_2^{ii}}g\lambda_{12}\bar{u}_1\gamma^\mu A_\mu^a T_a u_2 \\ & + \frac{Z_\lambda^{21}Z_1}{Z_2^{ii}}g\lambda_{21}\bar{u}_2\gamma^\mu A_\mu^a T_a u_1, \Big], \end{aligned} \tag{3}$$

where T_a are the eight Gell-Mann matrices in color space. Z_1^{ij}, Z_2^{ij}, and Z_3^{ij} are the vertex renormalization constant, quark field, and gauge boson field renormalization constant, respectively. The first four lines of action are the regular terms, which have SU(2) flavor symmetry in the case where u_1 and u_2 have the same mass. We introduced flavor mixing terms in the last four lines, which broke the symmetry. However, we let $\lambda_{ij} \to 0$ at the end of the calculations. This ensures that the items in the last four lines do not directly break our symmetry. If the flavor mixing effect persists after $\lambda_{ij} \to 0$, then SU(2) symmetry is broken dynamically. We need to introduce these terms, as mentioned earlier, to describe the process of flavor mixing coherently. Writing it out explicitly helps to deal more accurately with the effects of flavor mixing. This method of describing dynamic symmetry breaking can be summarized in the following formal statement [15]. First, we introduce the terms that describe symmetry breaking in the Lagrangian:

$$L_{\mathrm{SB}} = \lambda\bar{\psi}M\psi. \tag{4}$$

Here, $M \in g = \{T_a\}$ is the generator of the original symmetry group of the Lagrangian. The order parameter representing symmetry breaking can be expressed as its vacuum expectation value:

$$\Delta = \langle\bar{\psi}M\psi\rangle. \tag{5}$$

When we take $\lambda \to 0$, if $\Delta \neq 0$, then the symmetry T_a corresponding to $[T_a, M] \neq 0$ is broken. The corresponding susceptibility can be expressed as

$$\chi_\Delta = \lim_{\lambda\to 0}\frac{\Delta}{\lambda}. \tag{6}$$

A divergent susceptibility indicates that symmetry breaking has occurred. In our example, we take $M = T_1$, where T_1 is the

first generator of SU(2). Then, the order parameter is $\Delta \propto \langle \bar{u}_2 u_1 \rangle + \langle \bar{u}_1 u_2 \rangle$. Thus, when we take $\lambda_{ij} \to 0$, if there are still flavor mixing effects between u_1 and u_2, then dynamic symmetry breaking occurs, with the corresponding symmetry breaking pattern being SU(2) → SO(2). Because λ, which describes the flavor mixing effects, also needs to be renormalized, the renormalization constant Z_λ^{ij} is necessary. These renormalization constants are defined as follows:

$$u_i = \frac{1}{\sqrt{Z_2^{ii}}} u_{i0}, \quad A_\mu^a = \frac{1}{\sqrt{Z_3}} A_{\mu 0}^a,$$
$$g = \frac{Z_2^{ii}\sqrt{Z_3}}{Z_1} g^0, \quad \lambda_{ij} = \frac{\sqrt{Z_2^{11} Z_2^{22}}}{Z_\lambda^{ij}} \lambda_{ij}^0, \tag{7}$$

where the quantities with the index 0 represent the corresponding bare parameters, and the indexes take $\{i = 1, j = 2\}$ and $\{i = 2, j = 1\}$. By defining a flavor doublet $\psi \equiv \begin{pmatrix} u_1 \\ u_2 \end{pmatrix}$, $\bar{\psi} \equiv \psi^\dagger \Gamma^0 = \begin{pmatrix} \bar{u}_1 & \bar{u}_2 \end{pmatrix}$, where $\Gamma^\mu \equiv \begin{pmatrix} \gamma^\mu & 0 \\ 0 & \gamma^\mu \end{pmatrix}$, we can write the action in a compact form:

$$S = \int \mathrm{d}^4 x [\bar{\psi} Z_2 (i\not{\partial} - M)\psi + \bar{\psi} g Z_1 \Gamma^\mu A_\mu \psi - \frac{Z_3}{4} F_{\mu\nu} F^{\mu\nu} - \frac{Z_3}{2\xi} (\partial_\mu A^\mu)^2 \Big], \tag{8}$$

where

$$Z_1 = \begin{pmatrix} Z_1 & \frac{Z_1 Z_\lambda^{12} \lambda_{12}}{Z_2^{ii}} \\ \frac{Z_1 Z_\lambda^{21} \lambda_{21}}{Z_2^{ii}} & Z_1 \end{pmatrix},$$
$$Z_2(i\not{\partial} - M) = \begin{pmatrix} Z_2^{11}(i\not{\partial} - Z_m^{11} m_{11}) & Z_\lambda^{12}\lambda_{12}(i\not{\partial} - Z_m^{12} m_{12}) \\ Z_\lambda^{21}\lambda_{21}(i\not{\partial} - Z_m^{21} m_{21}) & Z_2^{22}(i\not{\partial} - Z_m^{22} m_{22}) \end{pmatrix}.$$

This form is not only simple, but its biggest advantage is that it helps to derive the DS equation uniformly and avoids complicated couplings among various flavors. Obviously, if $\lambda_{ij} = 0$ and $m_{11} = m_{22}$, the Lagrangian preserves SU(2) symmetry. In the discussion that follows, we keep $m_{11} = m_{22}$ and let $\lambda_{ij} \to 0$ at the end of the calculations. Finally, we find that the symmetry breaking effect still exists even if $\lambda_{ij} = 0$, indicating that the SU(2) symmetry at the Lagrangian level is broken dynamically.

For convenient numerical calculations, we switch to Euclidean space and write down the partition function as

$$Z_E = \int D(\bar{\psi}, \psi, A_\mu) \exp\Big\{ -\int \mathrm{d}^4 x \Big[\bar{\psi} Z_2 (\not{\partial} + M)\psi + \mathrm{i} g A_\mu \bar{\psi} Z_1 \Gamma^\mu \psi + \frac{Z_3}{4} F_{\mu\nu} F^{\mu\nu} + \frac{Z_3}{2\xi} (\partial_\mu A^\mu)^2 \Big] + \int \mathrm{d}^4 x [\bar{\psi}\eta + \bar{\eta}\psi + A_\mu J^\mu] \Big\}. \tag{9}$$

2.2. DS equations

Following [14], we derive the DS equation for quarks as

$$S^{-1}(p) = Z_2(\mathrm{i}\not{p} + M) + \mathrm{i} \int \frac{\mathrm{d}^4 k}{(2\pi)^4} g Z_1 \Gamma^\mu S(k) \Lambda_\varepsilon D_\mu^\varepsilon (p - k), \tag{10}$$

where S, D, and Λ represent the propagators of quarks, gauge bosons, and the complete vertex, respectively. It can be represented graphically as

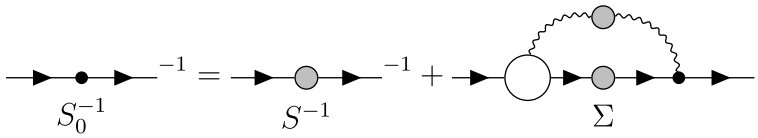

where S_0, S, and Σ represent the bare quark propagator, complete quark propagator, and self-energy of quarks, respectively. The gauge boson propagator is modeled by

$$g^2 D_{\mu\nu}(p) = D_{\mu\nu}^{\text{free}} p^2 G(p), \tag{11}$$

where free gauge boson propagator is

$$D_{\mu\nu}^{\text{free}} = \frac{1}{p^2}\left(g_{\mu\nu} - \frac{p_\mu p_\nu}{p^2} \right). \tag{12}$$

In this study, we use the Landau gauge. We take the bare vertex approximation and absorb g into the interaction model, thus

$$\Lambda^\mu = \Gamma^\mu = \begin{pmatrix} \gamma^\mu & 0 \\ 0 & \gamma^\mu \end{pmatrix}. \tag{13}$$

As mentioned previously, we are using a formulation that can self-consistently describe the flavor mixing process. Our basic idea is to think of the term describing the flavor mixing process as a renormalization flow. The actual physical correspondence of equation (3) can be obtained by taking $\lambda_{ij} = 0$. We view this as the definition of the theory at an energy scale ξ^2. At this scale, we cannot distinguish between $S_1 = S_0$ and $S_2 = S_0 + \lambda(\mu^2) S_\lambda$, where S_0 represents the first four lines in equation (3), whereas S_λ represents the other terms, and the flavor mixing term satisfies

$$\lambda(\mu^2 = \xi^2) = 0. \tag{14}$$

Thus, they should describe the same theory elsewhere below ξ^2. When we consider the effective theory at any other scale, the structure of S_2 changes significantly due to radiative corrections, and λ generates a nonzero value. This is just the flavor mixing effect we desired. The renormalization group can be used as a dynamic tool to include all effects of the full theory. Equation (14) defines the renormalization-group boundary condition for the full theory and can be viewed as our renormalization condition. For more related discussions, see, e.g. [16–19].

At the renormalization point ξ^2, we define the propagator as free. Thus, our renormalization condition can be written as

$$S(\xi^2)=\begin{pmatrix} -\mathrm{i}\not{\zeta}\dfrac{1}{\xi^2+m_{11}^2}+\dfrac{m_{11}}{\xi^2+m_{11}^2} & -\mathrm{i}\not{\zeta}a_{12}+b_{12} \\ -\mathrm{i}\not{\zeta}a_{21}+b_{21} & -\mathrm{i}\not{\zeta}\dfrac{1}{\xi^2+m_{11}^2}+\dfrac{m_{22}}{\xi^2+m_{22}^2} \end{pmatrix}, \quad (15)$$

where a_{12} and a_{21} have the dimension of $[M]^{-2}$, and b_{12} and b_{21} have the dimension of $[M]^{-1}$. Their values depend on λ_{ij} and m_{ij}. When $\lambda_{12}=\lambda_{21}=0$ and $m_{12}=m_{21}=0$, a_{12}, a_{21}, b_{12}, and b_{21} are also zero.

We can parameterize the quark propagator as

$$S=\begin{pmatrix} -\mathrm{i}\not{p}V_1(p^2)+S_1(p^2) & -\mathrm{i}\not{p}T_1(p^2)+R_1(p^2) \\ -\mathrm{i}\not{p}T_2(p^2)+R_2(p^2) & -\mathrm{i}\not{p}V_2(p^2)+S_2(p^2) \end{pmatrix}. \quad (16)$$

Substituting these into equation (10) and performing detailed derivations, we obtain eight nonlinear integral equations:

$$\begin{aligned} 1=&[Z_2^{11}Z_m^{11}m_{11}S_1(p^2)+Z_2^{11}p^2V_1(p^2) \\ &+Z_m^{12}m_{12}R_2(p^2)+Z_\lambda^{12}\lambda_{12}p^2T_2(p^2)] \\ &+\int\frac{\mathrm{d}^4k}{(2\pi)^4}G(p-k) \\ &\times\{3[S_1(k^2)S_1(p^2)+R_1(k^2)R_2(p^2)] \\ &+[V_1(k^2)V_1(p^2)+T_1(k^2)T_2(p^2)] \\ &\times\left[2p\cdot k+\frac{(p^2+k^2)p\cdot k-2p^2k^2}{(p-k)^2}\right]\Bigg\}. \end{aligned} \quad (17)$$

For brevity, we list only the first equation explicitly here, as shown in equation (17). The complete set of equations is listed in the appendix. All others are structurally similar to this one. For simplicity and solubility, we first consider the point interaction model [20], where $G(p)=G$ is a constant. Because of the rotational symmetry of the system, we can then write the four-dimensional integration as

$$\int\frac{\mathrm{d}^4k}{(2\pi)^4}=\frac{1}{8\pi^3}\int_0^{\Lambda^2}\mathrm{d}k^2k^2\int_0^{\pi}\mathrm{d}\theta\sin^2\theta, \quad (18)$$

where Λ is the regularization momentum truncation in the numerical calculations. In this case, we can solve semi-analytically and find that the result is almost unaffected by Λ. Specifically, when Λ^2 ranged from 10^5 to 10^{12}, the result changed by only a few ten-thousandths. Therefore, we ignored the influence of Λ and took it as a fixed value $\Lambda^2=10^7\,\mathrm{GeV}^2$. Looking closely at these formulas, we find that there is only one type of term involving angle in these integrations:

$$2pk\cos\theta+\frac{(p^2+k^2)pk\cos\theta-2p^2k^2}{p^2+k^2-2pk\cos\theta}\equiv f(p,k,\theta).$$

Thus, using the integration identity

$$\int_0^{\pi}\mathrm{d}\theta\sin^2\theta f(p,k,\theta)=-\frac{3\pi}{4}p^2+\frac{\pi}{4}\frac{p^4}{k^2}, \quad (19)$$

we can first integrate the angle integration out. We define

$$\begin{cases} \dfrac{G}{(8\pi)^3}\displaystyle\int\mathrm{d}k^2k^2V_1(k^2) &= CV_{11}, \\ \dfrac{G}{(8\pi)^3}\displaystyle\int\mathrm{d}k^2k^2\frac{1}{k^2}V_1(k^2) &= CV_{12}, \\ \dfrac{G}{(8\pi)^3}\displaystyle\int\mathrm{d}k^2k^2S_1(k^2) &= CS_{11}, \\ \dfrac{G}{(8\pi)^3}\displaystyle\int\mathrm{d}k^2k^2\frac{1}{k^2}S_1(k^2) &= CS_{12}, \end{cases} \quad (20)$$

and likewise for V_2, S_2, T_1, R_1, T_2, and R_2. We have then 16 parameters: CV_{ij}, CS_{ij}, CT_{ij}, and CR_{ij}, which are functionals of V_i, S_i, T_i, and R_i and are independent of p and k. As can be seen, the functions of p and k in these equations are decoupled so that by defining the functionals, we can collect the integrations to these parameters. Equation (17) now reads

$$\begin{aligned} 1=&[Z_2^{11}Z_m^{11}m_{11}S_1(p^2)+Z_2^{11}p^2V_1(p^2) \\ &+Z_m^{12}m_{12}R_2(p^2)+Z_\lambda^{12}\lambda_{12}p^2T_2(p^2)] \\ &+\frac{3\pi}{2}CS_{11}S_1(p^2)+\frac{3\pi}{2}CR_{11}R_2(p^2)-\frac{3\pi}{4}p^2CV_{11}V_1(p^2) \\ &+\frac{\pi}{4}p^4CV_{12}V_1(p^2)-\frac{3\pi}{4}p^2CT_{11}T_2(p^2)+\frac{\pi}{4}p^4CT_{12}T_2(p^2), \end{aligned} \quad (21)$$

and similarly for others (see the appendix). With the renormalization conditions defined at renormalization point ξ^2 by equation (15), we have

$$\begin{cases} V_1(\xi^2)=\dfrac{1}{\xi^2+m_{11}^2}, & S_1(\xi^2)=\dfrac{m_{11}}{\xi^2+m_{11}^2}, \\ V_2(\xi^2)=\dfrac{1}{\xi^2+m_{22}^2}, & S_2(\xi^2)=\dfrac{m_{22}}{\xi^2+m_{22}^2}, \\ T_1(\xi^2)=a_{12}, & R_1(\xi^2)=b_{12}, \\ T_2(\xi^2)=a_{21}, & R_2(\xi^2)=b_{21}. \end{cases} \quad (22)$$

As mentioned previously, a_{ij} and b_{ij} are related to λ_{ij} and m_{ij}. We take $\lambda_{12}=\lambda_{21}=0$ and $m_{12}=m_{21}=0$ now, and then $a_{12}=a_{21}=0$ and $b_{12}=b_{21}=0$. In this case, the renormalization condition corresponds to

$$S(\xi^2)=\begin{pmatrix} \dfrac{1}{\mathrm{i}\not{\zeta}+m_{11}} & 0 \\ 0 & \dfrac{1}{\mathrm{i}\not{\zeta}+m_{22}} \end{pmatrix}. \quad (23)$$

Using equations (21) and (22), we can solve the renormalization constants. Then, by substituting the renormalization constants back into equation (21), we get

$$\begin{cases} 1 = m_{ii}S_i(p^2) + \left(1 - \frac{\pi}{4}(\xi^2 - p^2)CV_{i2}\right)p^2 V_i(p^2) - \frac{\pi}{4}(\xi^2 - p^2)p^2 CT_{i2}T_j(p^2), \\ 0 = m_{ii}R_i(p^2) + \left(1 - \frac{\pi}{4}(\xi^2 - p^2)\right)p^2 CV_{i2}T_i(p^2) - \frac{\pi}{4}(\xi^2 - p^2)p^2 CT_{i2}V_j(p^2), \\ 0 = -m_{ii}V_i(p^2) + \left(1 - \frac{\pi}{4}(\xi^2 - p^2)\right)CV_{i2}S_i(p^2) - \frac{\pi}{4}(\xi^2 - p^2)CT_{i2}R_j(p^2), \\ 0 = -m_{ii}T_i(p^2) + \left(1 - \frac{\pi}{4}(\xi^2 - p^2)\right)CV_{i2}R_i(p^2) - \frac{\pi}{4}(\xi^2 - p^2)CT_{i2}S_j(p^2), \end{cases} \tag{24}$$

for $\{i = 1, j = 2\}$ and $\{i = 2, j = 1\}$. It is found that only $\{CV_{12}, CV_{22}, CT_{12}, CT_{22}\}$ appear in the final equations. Luckily, these equations are linear for $\{V_i(p^2), S_i(p^2), T_i(p^2), R_i(p^2)\}$, and $\{CV_{12}, CV_{22}, CT_{12}, CT_{22}\}$ are just constants that are independent of momentum so that we can solve them analytically. Even so, they are still very tedious. Therefore, we abbreviate them as

$$\begin{cases} V_i(p^2;\, CV_{12}, CV_{22}, CT_{12}, CT_{22}), \\ S_i(p^2;\, CV_{12}, CV_{22}, CT_{12}, CT_{22}), \\ T_i(p^2;\, CV_{12}, CV_{22}, CT_{12}, CT_{22}), \\ R_i(p^2;\, CV_{12}, CV_{22}, CT_{12}, CT_{22}). \end{cases} \tag{25}$$

If we substitute the functions in equation (25) back to the definition in equation (20), we can determine the four variables numerically. Once this is done, we have $\{CV_{12}, CV_{22}, CT_{12}, CT_{22}\}$, from which we obtain $\{V_i, S_i, T_i, R_i\}$, allowing us to derive all other necessary quantities.

Because of the hermiticity of the Lagrangian, we have

$$S_{ij}^{-1}(p) = \gamma^{0\dagger}S_{ij}^{\dagger}(p)\gamma^0, \tag{26}$$

which was given in [13]. Thus the solutions must satisfy $T_1(p^2) = T_2(p^2)$ and $R_1(p^2) = R_2(p^2)$. We take these relations as conditions in the following discussion. Therefore, we have totally three unknown variables $\{CV_{12}, CV_{22}, CT_2 \equiv CT_{12} = CT_{22}\}$, which can be organized in a three-dimensional Cartesian coordinate.

3. Numerical result

3.1. Structure of the solutions

As mentioned previously, one solution can be parameterized by three variables: $\{CV_{12}, CV_{22}, CT_2\}$. We can represent these three variables in a three-dimensional space, where each solution is presented as a point. As shown in figure 1, there are infinitely many solutions, as expected, due to the original Lagrangian SU(2) symmetry. Apparently, these solutions can be classified into three groups, each forming an ellipse with an eccentricity $e = \frac{\sqrt{2}}{2}$. This explains why we used the point interaction model. In this model, we can solve the DS equation semi-analytically. Most importantly, only three parameters are needed to parameterize the solutions, providing a solid foundation for studying the structure of the solutions. Although we could choose other more realistic interaction models, solving the equations numerically would be necessary, making it difficult to reveal the structure of the solutions without advanced knowledge.

We can define an SO(2) rotation as

$$\begin{pmatrix} u'_1 \\ u'_2 \end{pmatrix} = \begin{pmatrix} \cos\theta' & -\sin\theta' \\ \sin\theta' & \cos\theta' \end{pmatrix}\begin{pmatrix} u_1 \\ u_2 \end{pmatrix}. \tag{27}$$

It is a rotation by θ' in the flavor space $\psi = \begin{pmatrix} u_1 \\ u_2 \end{pmatrix}$. This rotation acts on the propagator as

$$\begin{aligned} S \to S' = &\begin{pmatrix} \cos\theta' & -\sin\theta' \\ \sin\theta' & \cos\theta' \end{pmatrix} \\ &\times\begin{pmatrix} -\mathrm{i}\not{p}V_1(p^2) + S_1(p^2) & -\mathrm{i}\not{p}T(p^2) + R(p^2) \\ -\mathrm{i}\not{p}T(p^2) + R(p^2) & -\mathrm{i}\not{p}V_2(p^2) + S_2(p^2) \end{pmatrix} \\ &\times\begin{pmatrix} \cos\theta' & \sin\theta' \\ -\sin\theta' & \cos\theta' \end{pmatrix}. \end{aligned} \tag{28}$$

Obviously, the rotations of the scalar and vector parts do not mix; therefore, the two parts rotate independently. Combining the definition in equation (20), we find that the rotation of V_i and T is equivalent to the rotation of CV_{i2} and CT_2, that is, equation (28) is equivalent to

$$\begin{aligned} \begin{pmatrix} CV'_{12} & CT'_2 \\ CT'_2 & CV'_{22} \end{pmatrix} = &\begin{pmatrix} \cos\theta' & -\sin\theta' \\ \sin\theta' & \cos\theta' \end{pmatrix} \\ &\times\begin{pmatrix} CV_{12} & CT_2 \\ CT_2 & CV_{22} \end{pmatrix}\begin{pmatrix} \cos\theta' & \sin\theta' \\ -\sin\theta' & \cos\theta' \end{pmatrix}. \end{aligned} \tag{29}$$

Thus, we see that θ', as a rotation in the flavor space, can also act on $\{CV_{i2}, CS_{i2}, CT_2, CR_2\}$, provided that they are organized into a 2×2 parameter matrix as $P_{\mathrm{M}} \equiv \begin{pmatrix} CV_{12} & CT_2 \\ CT_2 & CV_{22} \end{pmatrix}$. The preceding discussion shows that we can diagonalize the 2×2 propagator or mass matrix by an SO(2) rotation, and the rotation in equation (29) of the parameter matrix P_{M} is exactly the rotation that diagonalizes the propagator.

We have shown that a rotation of θ' in the flavor space corresponds to a rotation acting on the parameter matrix P_{M}. We now discuss the rotation on an ellipse formed by a set of solutions of the DS equation, as shown in figure 2.

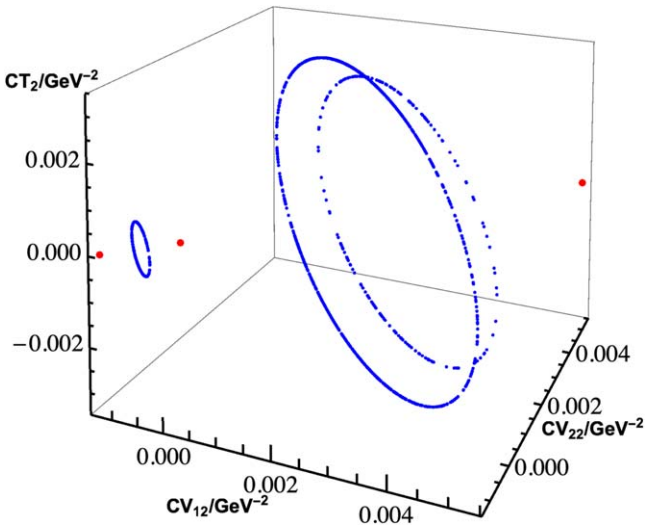

Figure 1. Structure of the obtained gap equation solutions. These solutions were solved using the following parameters: $G = 1000\ \text{GeV}^{-2}$, $m_{11} = m_{22} = 50\ \text{GeV}$, and $\xi^2 = 1000\ \text{GV}^2$. There are two isolated (red) points on both sides of each ellipse, which are solutions without mixing between the two flavor hyperquarks. There are three points in total. These points do not break the SU(2) symmetry.

The ellipse shown in figure 2 can be described by

$$\left(CV_{12} - \frac{c_0}{2}\right)^2 + \left(CV_{22} - \frac{c_0}{2}\right)^2 + 2CT_2^2 = a_0^2, \tag{30a}$$

$$CV_{12} + CV_{22} = c_0, \tag{30b}$$

where we have used the conclusion that the eccentricity of each ellipse is $\frac{\sqrt{2}}{2}$, a_0 describes the size of the ellipse, and c_0 describes the position of the ellipse. The coordinates of the point with angle θ are

$$\begin{cases} CV_{12} = \dfrac{c_0}{2} - \dfrac{a_0 \tan\theta}{\sqrt{4 + 2\tan^2\theta}}, \\ CV_{22} = \dfrac{c_0}{2} + \dfrac{a_0 \tan\theta}{\sqrt{4 + 2\tan^2\theta}}, \\ CT_2 = \dfrac{a_0}{\sqrt{2 + \tan^2\theta}}. \end{cases} \tag{31}$$

The rotation of θ in terms of the parameter matrix can be represented as

$$\begin{pmatrix} \frac{c_0}{2} & \frac{a_0}{\sqrt{2}} \\ \frac{a_0}{\sqrt{2}} & \frac{c_0}{2} \end{pmatrix}_{\theta=0} \xrightarrow{\theta} \begin{pmatrix} \frac{c_0}{2} - \frac{a_0\tan\theta}{\sqrt{4+2\tan^2\theta}} & \frac{a_0}{\sqrt{2+\tan^2\theta}} \\ \frac{a_0}{\sqrt{2+\tan^2\theta}} & \frac{c_0}{2} + \frac{a_0\tan\theta}{\sqrt{4+2\tan^2\theta}} \end{pmatrix}. \tag{32}$$

We substitute the rotation of θ' in the flavor space into equation (29) and obtain that the rotation of θ' is represented by the parameter matrix as

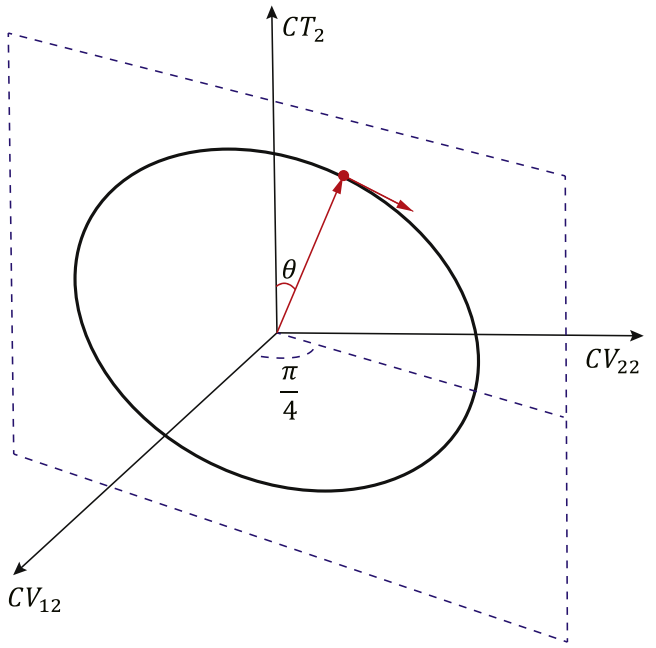

Figure 2. Schematic of the elliptical structure of the solutions. A rotation by angle θ in this ellipse is associated with an SO(2) transformation in the flavor space. The plane of the ellipse has an angle of $\frac{\pi}{4}$ with the CV_{12} and CV_{22} axes. Note that the origin of the coordinate system in the figure is not necessary at (0, 0, 0). The point with $CV_{12} = CV_{22}$ ($\theta = 0$ or $\theta = \pi$) is a fixed point of SU(2). The points with $\theta = \frac{\pi}{2}$ and $\theta = \frac{3\pi}{2}$ correspond to the diagonalized points.

$$\begin{pmatrix} \frac{c_0}{2} & \frac{a_0}{\sqrt{2}} \\ \frac{a_0}{\sqrt{2}} & \frac{c_0}{2} \end{pmatrix}_{\theta'=0} \xrightarrow{\theta'} \begin{pmatrix} \frac{c_0}{2} - \frac{a_0}{\sqrt{2}}\sin 2\theta' & \frac{a_0}{\sqrt{2}}\cos 2\theta' \\ \frac{a_0}{\sqrt{2}}\cos 2\theta' & \frac{c_0}{2} + \frac{a_0}{\sqrt{2}}\sin 2\theta' \end{pmatrix}. \tag{33}$$

Comparing the preceding two expressions, we see that the two rotations can correspond one by one, and the relation between them is

$$\tan 2\theta' = \frac{\tan\theta}{\sqrt{2}}. \tag{34}$$

As θ varied on the ellipse, the behavior of the parameters characterizing the solutions changed, as shown in figure 3. It can be seen that as θ changed from 0 to $\frac{\pi}{2}$, V_1 and S_1 gradually separated from V_2 and S_2, respectively, indicating that the mass function changed from degeneracy to splitting. T and R gradually changed from finite values to zero, indicating that the flavor mixing effect gradually disappeared. According to the changing behavior in the figure and the specific expressions of $T(p^2)$ and $R(p^2)$ for the flavor mixing terms, it can be shown that when a point is rotated to the endpoint of the ellipse, the off-diagonal term of the propagator becomes zero at all momenta, which corresponds to the diagonalization of the propagator.

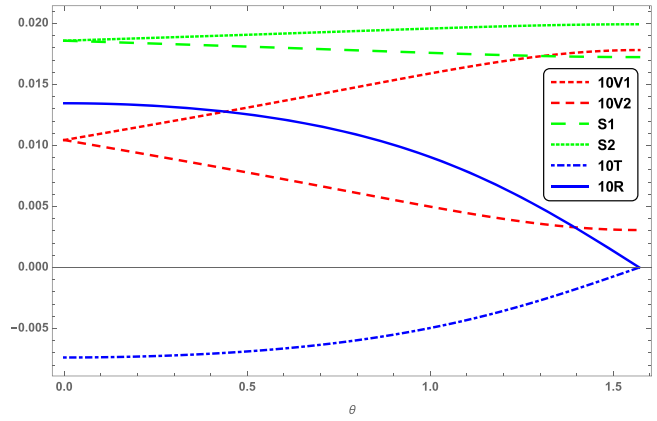

Figure 3. Behavior of the key parameters that characterize the solutions as θ went from 0 to π. The momentum was taken at $p^2 = 15$. (We are not showing them at zero momentum because there is no difference between S_1 and S_2 at zero momentum.) For clarity, V_1, V_2, T, and R are displayed with a tenfold increase. Dimensional quantities are in units of GeV.

We can see that an SO(2) rotation in the flavor space $\psi = \begin{pmatrix} u_1 \\ u_2 \end{pmatrix}$ is equivalent to a rotation on the ellipse in the solution space. It can also be shown that if we transform along the other two directions of the SU(2) group, the points in the corresponding solution space will move out of the ellipse, making the transformed solution no longer a solution to the DS equation. Our original Lagrangian had SU(2) symmetry, and the DS equation derived from this Lagrangian also had SU(2) symmetry. If we perform SO(2) rotation in the flavor space, the solution needs to be transformed accordingly. The previous discussion showed that the solution after SO(2) transformation moves on the ellipse, not leaving it, and thus remains a solution to the DS equation. Therefore, SO(2) symmetry is preserved. However, if we apply an SU(2) transformation in a direction other than SO(2), the solution moves out of the ellipse, meaning the transformed solution is no longer a solution to the DS equation. In other words, the original Lagrangian has SU(2) symmetry, but its solution does not retain SU(2) symmetry, indicating that the SU(2) symmetry is dynamically broken to SO(2). There are two exceptions: points where $CV_{12} = CV_{22}$ ($\theta = 0$ or $\theta = \pi$). These two points remain fixed under the transformation of the other two directions of the SU(2) group, thereby maintaining SU(2) symmetry. From figure 1, we can see that there are three isolated points with the property $CV_{12} = CV_{22}$, indicating that they also retain SU(2) symmetry.

It is also worth mentioning that the points on the ellipse that are not at $CT_2 = 0$ have nonzero $R(p^2)$ and $T(p^2)$, indicating flavor change effects, but they are not mass eigenstates and therefore not physical states. It is necessary to say something about the effect of the flavor change. Without diagonalizing the solution, these solutions exhibit flavor change effects but are not physical states and cannot be directly observed. By the basic principle of measurement for quantum systems, observable states are mass eigenstates, which are the states after diagonalization. After diagonalization, the flavor change effect disappeared, indicating that the flavor change effects are only 'intermediate states'. It has physical consequences (such as leading to mass splitting) but does not appear in the final physical states. We can obtain the physical states by diagonalizing the propagator or mass matrix through the rotation in equation (28). Diagonalizing the propagator is equivalent to diagonalizing the parameter matrix P_{M}, which is equivalent to rotating a point on the ellipse in figure 2 to its endpoint. The fact that the eccentricity of each ellipse is fixed at $e = \frac{\sqrt{2}}{2}$ is significant because it ensures that regardless of the solution we choose, the diagonalized physical state will be the same, and the flavor change effect can be eliminated. This shows that every point on the ellipse corresponds to the same physical state. Thus, an entire ellipse can be mapped to one physical state, establishing a one-to-one correspondence between ellipses and physical states. If we consider the different excited states of the hyperquark as particles of different masses, then each ellipse corresponds to one particle. Therefore, the physical states corresponding to the three ellipses can be considered as three quarks with the same quantum number but different masses (m_1, m_2, and m_3). The residual SO(2) symmetry after the SU(2) symmetry is broken to SO(2) is important because it ensures that the flavor change effects can be eliminated and do not appear in the final physical state.

3.2. Mass splitting and spectrum

Because the eccentricity of each ellipse is fixed, only two parameters are required to characterize them, namely a_0 and c_0, as shown by the ellipse equations (30). We only need to know one point on the ellipse to determine a_0 and c_0. The parameter matrix can then be diagonalized to

$$\begin{pmatrix} CV_{12} & CT_2 \\ CT_2 & CV_{12} \end{pmatrix} \longrightarrow \begin{pmatrix} \frac{c_0 + \sqrt{2}a_0}{2} & 0 \\ 0 & \frac{c_0 - \sqrt{2}a_0}{2} \end{pmatrix}. \tag{35}$$

Its corresponding diagonalized propagator is

$$S = \begin{pmatrix} \mathrm{i}\not{p} V_1(p^2) + S_1(p^2) & 0 \\ 0 & \mathrm{i}\not{p} V_2(p^2) + S_2(p^2) \end{pmatrix}, \tag{36}$$

where

$$\begin{cases} V_1(p^2) = \dfrac{1 + \frac{\pi}{4}\frac{c_0+\sqrt{2}a_0}{2}(p^2 - \xi^2)}{m_{11}^2 + p^2\left(1 + \frac{\pi}{4}\frac{c_0+\sqrt{2}a_0}{2}(p^2 - \xi^2)\right)^2}, \\ S_1(p^2) = \dfrac{m_{11}}{m_{11}^2 + p^2\left(1 + \frac{\pi}{4}\frac{c_0+\sqrt{2}a_0}{2}(p^2 - \xi^2)\right)}, \\ M_1(p^2) = \dfrac{S_1(p^2)}{V_1(p^2)} = \dfrac{m_{11}}{1 + \frac{\pi}{4}\frac{c_0+\sqrt{2}a_0}{2}(p^2 - \xi^2)}, \end{cases} \tag{37}$$

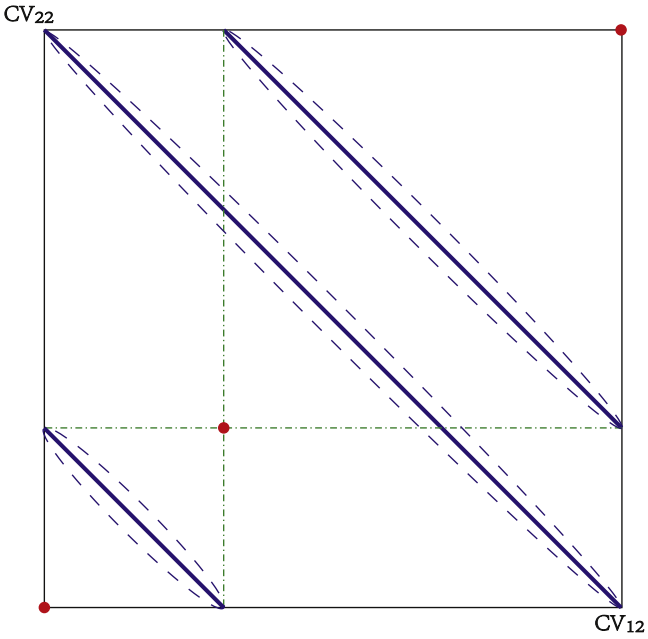

Figure 4. Top view of the solutions, with each diagonal line representing an ellipse. Each ellipse has two diagonalized states (physical states) corresponding to the two endpoints of the ellipse. The six physical states of the three ellipses are repeated in pairs, giving a total of three different physical states that can be represented equivalently (numerically) by the larger (red) dots in the figure.

$$\begin{cases} V_2(p^2) = \dfrac{1+\frac{\pi}{4}\frac{c_0-\sqrt{2}a_0}{2}(p^2-\xi^2)}{m_{22}^2+p^2\left(1+\frac{\pi}{4}\frac{c_0-\sqrt{2}a_0}{2}(p^2-\xi^2)\right)^2}, \\ S_2(p^2) = \dfrac{m_{22}}{m_{22}^2+p^2\left(1+\frac{\pi}{4}\frac{c_0-\sqrt{2}a_0}{2}(p^2-\xi^2)\right)}, \\ M_2(p^2) = \dfrac{S_1(p^2)}{V_1(p^2)} = \dfrac{m_{22}}{1+\frac{\pi}{4}\frac{c_0-\sqrt{2}a_0}{2}(p^2-\xi^2)}. \end{cases} \tag{38}$$

As expected, because $T = R = 0$ after diagonalization, the off-diagonal element describing the flavor mixing effect is no longer present.

From figure 1, we can see that three different sets of solutions form three ellipses. These ellipses have subtle interrelationships worthy of a detailed discussion. Figure 4 shows the top view along the CT_2 direction, where each ellipse is oriented in the same way, parallel to each other, and extends from the top left to the bottom right (135 degrees), all embedded in the same square. Notably, the left end of the uppermost ellipse shares the same abscissa as the right end of the lowermost ellipse, and the right end of the uppermost ellipse shares the same ordinate as the left end of the lowermost ellipse, as illustrated by the green dotted lines in figure 4. In fact, the six endpoints of the three ellipses have paired horizontal and vertical coordinates. Although there are 12 coordinates in total, only six are distinct because of these repetitions. Additionally, from the elliptic equations (30), we can see that the center point of each ellipse lies on the line $CV_{12} = CV_{22}$. Thus, these ellipses have reflective symmetry with respect to the line of $x = y$ (45 degrees). Taking this into account, there are actually only three distinct horizontal and vertical coordinates for the three ellipses, which are numerically equivalent to the larger red dots in figure 4.

In the previous section, we discussed that a nonzero CT_2 implies nonzero off-diagonal terms of the propagator, that is, it represents the flavor mixing effect between the hyperquarks. However, the flavor mixing effect disappears with the diagonalization process and does not manifest in the end. It only affects the splitting size of the eigenstate of mass, as shown in equation (35). Flavor mixing effects and dynamic chiral symmetry breaking (DCSB) share many similarities. Both are non-perturbative dynamic effects related to symmetry breaking: DCSB involves the breaking of chiral symmetry, whereas flavor mixing effects involve the breaking of SU(2) flavor symmetry. Additionally, both phenomena occur only when the interaction strength exceeds a certain critical value. We can use the size of the ellipse, a_0, or the value of CT_2 with the maximum flavor mixing effect to describe the strength of the flavor mixing effect. Its relationship with the strength of the interaction is shown in figure 5(a). In figure 5, we also include the behavior of solutions without flavor mixing effects. The blue solid dots represent the corresponding data of solutions with flavor mixing effects (corresponding to the blue ellipses in figures 1 and 4), whereas the red hollow diamonds represent the corresponding data of solutions without flavor mixing effects (corresponding to the larger red dots in figures 1 and 4). It can be seen that there is a critical interaction strength, and the flavor mixing effect only appears when the interaction strength exceeds this threshold. As the interaction strength decreases toward the critical strength, two ellipses of the three sets of solutions gradually approach each other (as shown in figure 5(b), where c_0 represents the position of the ellipse) and approach the same size (as shown in figure 5(a), where a_0 represents the size of the ellipse), while the size of the other ellipse approaches zero. Figure 6 shows the changes in these ellipses under several different interaction strengths, intuitively reflecting the aforementioned trends. From figure 5(b), it can also be seen that the center of each ellipse is always in the middle of a pair of solutions without flavor mixing effects. These are consistent with the previous descriptions of the relationships between the three ellipses. Additionally, according to the changes in a_0 and c_0 in the figure, it can be seen that when the interaction strength approaches zero, both a_0 and c_0 also approach zero. According to equations (37) and (38), we get $M_1 = M_2 = m_{11} = m_{22}$, which also matches our expectations. The behavior of the diagonalized CV_{12} (or CV_{22}) with the interaction strength is shown in figure 5(c). As we can see, there are really only three different CV_{12} (or CV_{22}). Figure 5(d) shows the behavior of the diagonalized chiral condensation with the strength of the interaction, which reflects the splitting of the mass eigenstates.

In the chiral limit, nonzero chiral condensation is the cause of the dynamic mass. Similarly, in the limit of $\lambda_{ij} = 0$ in the Lagrangian (3), a nonzero mixing condensation is the cause of flavor mixing. The mixing condensation can be

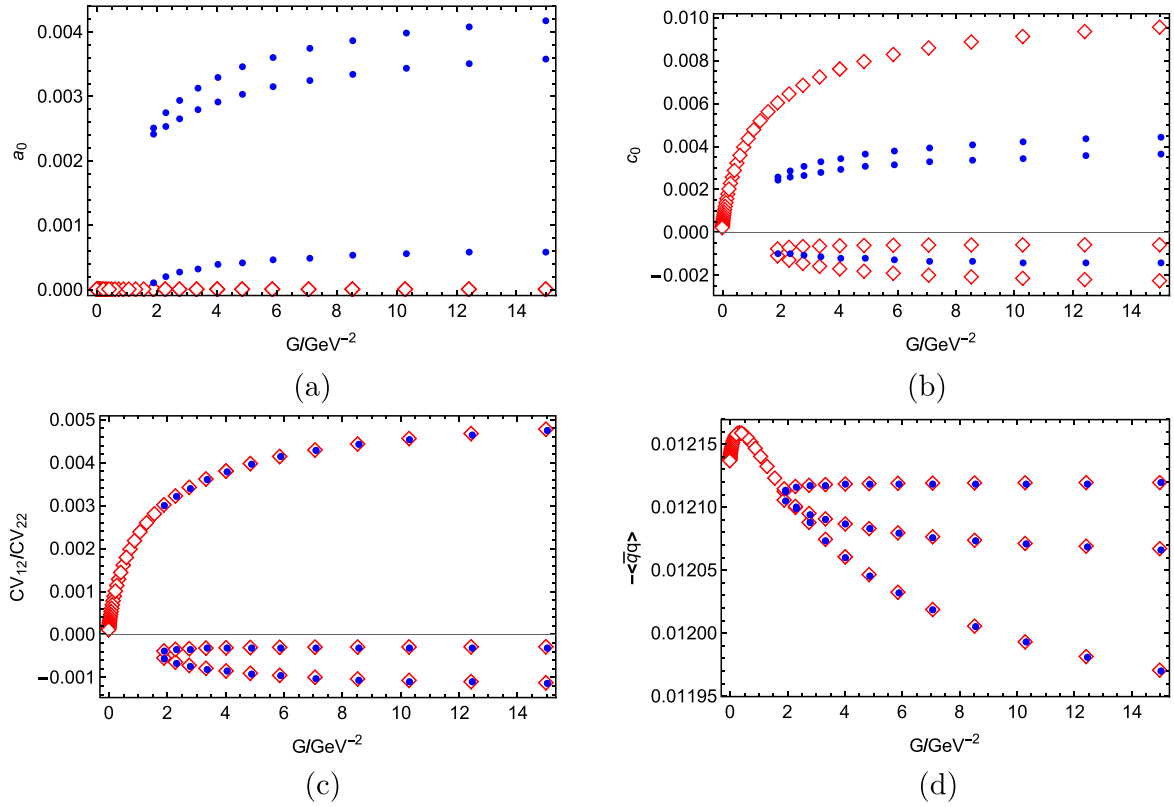

Figure 5. Behavior of various parameters with the interaction strength. The other parameters are the same as those shown in figure 1: $m_{11} = m_{22} = 50$ GeV and $\xi^2 = 1000$ GV^2. The blue solid dots represent the corresponding data of solutions with flavor mixing effects (corresponding to the blue ellipses in figures 1 and 4), whereas the red hollow diamonds represent the corresponding data of solutions without flavor mixing effects (corresponding to the red solid dots in figures 1 and 4). The behavior of (a) a_0, (b) c_0, (c) diagonalized CV_{12} or CV_{22} (corresponding to the values at the endpoints of the ellipse), and (d) regular condensation $-\langle\bar{q}_1 q_1\rangle$ or $-\langle\bar{q}_2 q_2\rangle$ with interaction strength G. The regular condensation was taken at the diagonalized points (corresponding to the endpoints of the ellipse).

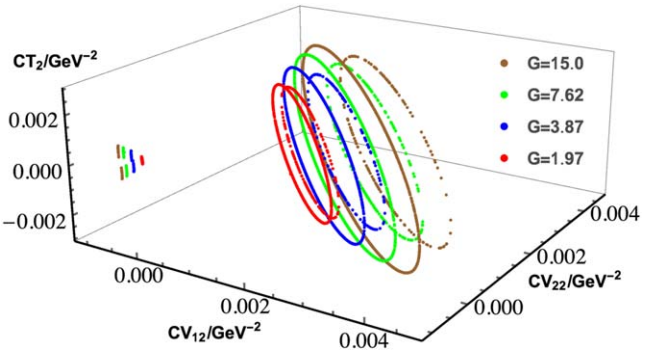

Figure 6. Behavior of the solutions of the DS equations with varying interaction strength G. The other parameters are the same as those shown in figure 1: $m_{11} = m_{22} = 50$ GeV and $\xi^2 = 1000$ GV^2.

expressed as a trace of its corresponding mixed propagator:

$$-\langle\bar{q}_1 q_2\rangle = \frac{32\pi N_c}{G} CR_{11},$$
$$-\langle\bar{q}_2 q_1\rangle = \frac{32\pi N_c}{G} CR_{21}. \quad (39)$$

Here, q represents the hyperquarks. It can serve as an order parameter describing symmetry breaking from SU(2) to SO(2). The behavior of these quantities with varying interaction strength is shown in figure 7. In this figure, the line where the mixing condensation (taking the value at the highest point of the ellipse, which represents the maximum mixing effect) is always zero (indicated by red diamonds) represents solutions without flavor mixing effects, corresponding to the larger red dots in figures 1 and 4, which exist at all interaction strengths. It can be seen that the mixing condensation is initially zero, maintaining SU(2) symmetry. When the interaction strength reaches a critical value, multiple solutions start to appear, splitting into nonzero mixing condensations, indicating the onset of flavor mixing effects. At this point (for these nonzero solutions), the SU(2) symmetry is broken. To illustrate this better, we can make an analogy with the case of DCSB in the chiral limit. Solutions where the mixing condensation is always zero are similar to 'Wigner solutions', maintaining symmetry, whereas solutions with nonzero mixing condensation are similar to 'Nambu solutions', breaking symmetry. In summary, whether the usual chiral condensation, mixing condensation, or other parameters such as a_0, they all have only one trivial solution below the critical strength. Nontrivial solutions start to appear at the critical value. This is also why it is said that the breaking from SU(2) to SO(2) mentioned earlier is due to dynamic symmetry breaking.

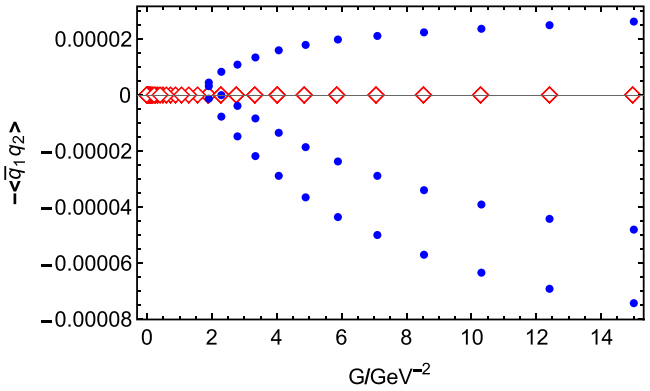

Figure 7. Behavior of the mixing condensate $-\langle\bar{q}_1 q_2\rangle$ or $-\langle\bar{q}_2 q_1\rangle$ with interaction strength G. The mixing condensate was taken as the value at the point with the maximum mixing effect, which is the highest point of the ellipse. The other parameters are the same as those shown in figure 1, taken as $m_{11} = m_{22} = 50$ GeV and $\xi^2 = 1000\,\mathrm{GV}^2$. The blue solid dots represent the corresponding data of solutions with flavor mixing effects (corresponding to the blue ellipses in figures 1 and 4), whereas the red hollow diamonds represent the corresponding data of solutions without flavor mixing effects (corresponding to the larger red dots in figures 1 and 4).

Based on the previous discussion about the structure of the solutions and their interrelations, we know that each solution on an ellipse can be diagonalized to obtain two different mass eigenvalues. Because of their subtle relationships, there are three distinct mass eigenvalues. According to [21], one may interpret either the different solutions of a gap equation or the different propagator poles of one solution as particles of different generations. Thus, we can obtain three-generation quark masses from the diagonalized propagator.

When $\xi^2 = 4.52 \times 10^4\ \mathrm{GeV}^2$, $G = 2.88 \times 10^{-6}\,\mathrm{GeV}^{-2}$, and $m_{11} = m_{22} = 2.15$ MeV, the three diagonalized solutions (corresponding to the three red points in figure 4) are $(2.812 \times 10^{-5}, 2.812 \times 10^{-5}, 0)$, $(2.817 \times 10^{-5}, 2.817 \times 10^{-5}, 0)$, and $(3.223 \times 10^{-7}, 3.223 \times 10^{-7}, 0)$ in units of GeV^{-2}. Corresponding to one ellipse in the figure, after the diagonalization, the propagator structure functions and mass functions under this group of parameters are shown in figure 8. From these mass functions, we can obtain the constituent mass and current mass. We take the mass value at 2 GeV as the current mass. However, it is worth noting that the definition of the current masses of heavy quarks is slightly different in the next section. We then get $m_u = 2.17$ MeV, $m_c = 1.27$ GeV, and $m_t = 171$ GeV. As we can see, the mass functions are large but finite in the infrared region and approach zero in the ultraviolet region. Moreover, their masses exhibit significant splitting as we expected.

After diagonalization, the two physical states have different masses, i.e. mass splitting. At this point, because the masses of the two particles are different, they no longer have SU(2) symmetry, not even SO(2) symmetry. Therefore, is the symmetry breaking chain SU(2) → SO(2) or SU(2) → 0? This question is worth exploring. In fact, during spontaneous symmetry breaking, the symmetry is not truly broken but rather hidden. The original symmetry still strongly constrains the system, but it no longer manifests directly and exists in a

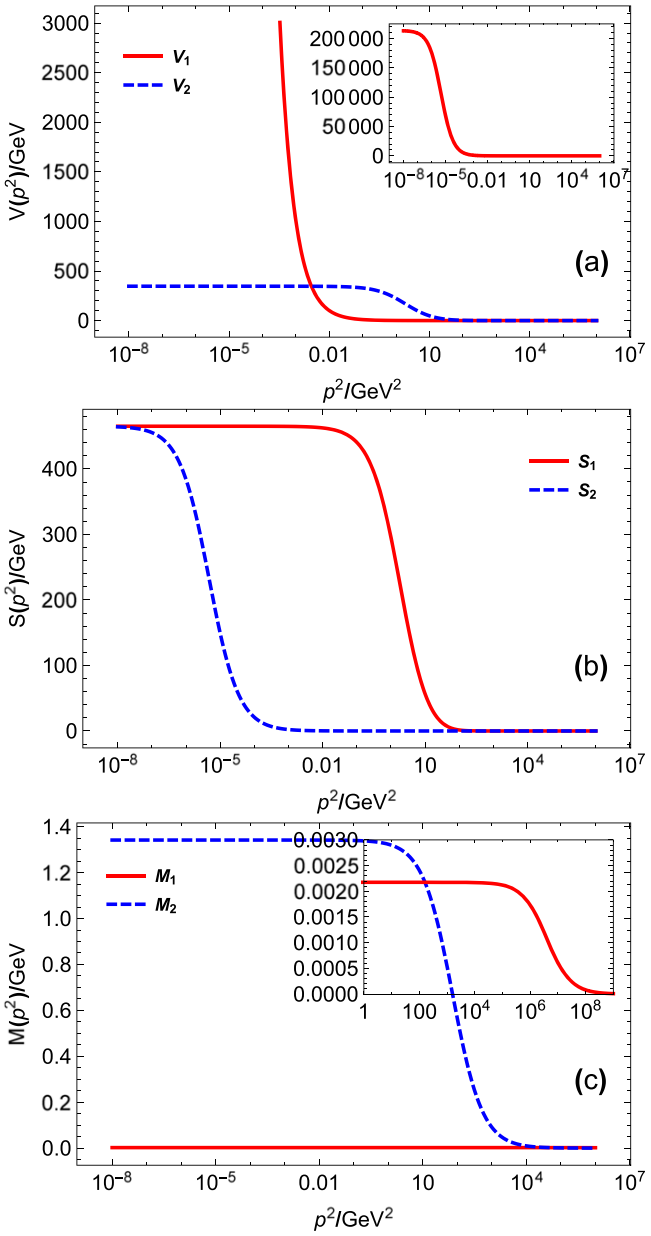

Figure 8. Diagonalized propagator structure functions. The parameters are taken as $\xi^2 = 4.52 \times 10^4\ \mathrm{GeV}^2$, $G = 2.88 \times 10^{-6}\,\mathrm{GeV}^{-2}$, and $m_{11} = m_{22} = 2.15$ MeV. The two color lines correspond to the two different solutions obtained by diagonalization. (a) Vector structure functions $V_i(p^2)$. (b) Scalar structure functions $S_i(p^2)$. (c) Mass functions $M_i(p^2)$.

nonlinear representation (see [6] for a detailed discussion). Similarly, after choosing a specific state, we no longer see the SO(2) symmetry, but it remains hidden. The entire system still possesses SO(2) symmetry. What we correspond with the particle is not a specific state but a higher level 'all' and 'mixed' state, i.e. the entire ellipse. It can be any point on the ellipse, but it is not any specific point. Our understanding that the entire ellipse corresponds to one particle (rather than one point corresponding to one particle) ensures this SO(2) symmetry. In other words, the different generations of quarks resulting from mass splitting are mixed states of hyperquarks. When we look from the perspective of quarks (e.g. u and c

quarks), they do not have SO(2) symmetry, but when we still look from the perspective of hyperquarks (e.g. u_1 and u_2), they have SO(2) symmetry. We certainly cannot view the hyperquark symmetry from the quark's perspective. (Both SU(2) and SO(2) symmetries are hyperquark symmetries.)

3.3. Numerical results with a more realistic interaction model

Although the point interaction model described previously clearly shows the structure of the solutions, it has some problems. First, the masses $m_{11} = m_{22} \neq 0$ cannot be set to zero because of infrared divergence. Second, the mass function may be divergent at some scale and becomes negative. As we can see, the denominator of the mass function is $1 + \frac{\pi}{4}\frac{c_0 - \sqrt{2}a_0}{2}(p^2 - \xi^2)$, so if $c_0 - \sqrt{2}a_0 > \frac{8}{\pi}\xi^2$, the mass function will diverge at $p^2 = \xi^2 - \frac{8}{\pi(c_0 - \sqrt{2}a_0)}$ and becomes negative below it. Lastly, higher-generation quarks, such as the c quark, always have more mass, whereas lower-generation quarks, such as the u quark, have less mass at the same momentum scale, and the constituent masses of heavy flavor quarks are not much different from their current masses, whereas the constituent masses of light flavor quarks are significantly greater than their current masses [22]. However, the mass functions we obtained from the point interaction model lacked these expected features.

These problems arise from the inappropriate interaction model. In our point interaction model, the interaction function $G(p)$ is constant, whereas the dominant strong interaction is asymptotically free. Therefore, we should take a more realistic interaction model. Different interaction models are embodied in different $G(p^2)$. We take

$$G(p^2) = \frac{4}{3}G_1(p^2) + G_2(p^2), \tag{40}$$

where $\frac{4}{3}$ arises from the sum of color matrices, and

$$G_1(p^2) = \frac{8\pi^2}{\omega^4}De^{-\frac{p^2}{\omega^2}} \tag{41}$$

is the infrared constant model (usually referred to as the QC model) [23] to describe the strong interaction, whereas

$$G_2(p^2) = \frac{e^2}{p^2 + \mu^2}, \tag{42}$$

models the remaining interactions, including the electromagnetic interaction. Because we used a more complex model, we were only able to carry out purely numerical calculations now. Thanks to the previous point interaction model, we have understood the basic structure of the solutions, which makes numerical calculations less difficult. Using the same method as before, we can address the current numerical problems with a simple expansion. It is proven that the preceding discussions on the basic structures of the solutions are also valid under the current model.

An example of the mass functions obtained under a set of typical parameters is shown in figure 9.

So far, we have only discussed up-type quarks. The same calculations and discussions can be done for down-type quarks. The strong interaction parts of the up- and down-type quarks are the same, but they have different charges and weak charges. Therefore, for the down-type part, we used the same $G_1(p^2)$ (i.e. the same D and ω) as the up-type part, but used different parameters for $G_2(p^2)$ (different G_2). As mentioned earlier, according to the viewpoint in [21], we can interpret the different solutions of the gap equation as different generations of particles. Therefore, we can correspond the three mass functions to the three generations of quarks, thereby obtaining the mass spectra of the three generations of quarks. If we accept this correspondence, we can use the masses of

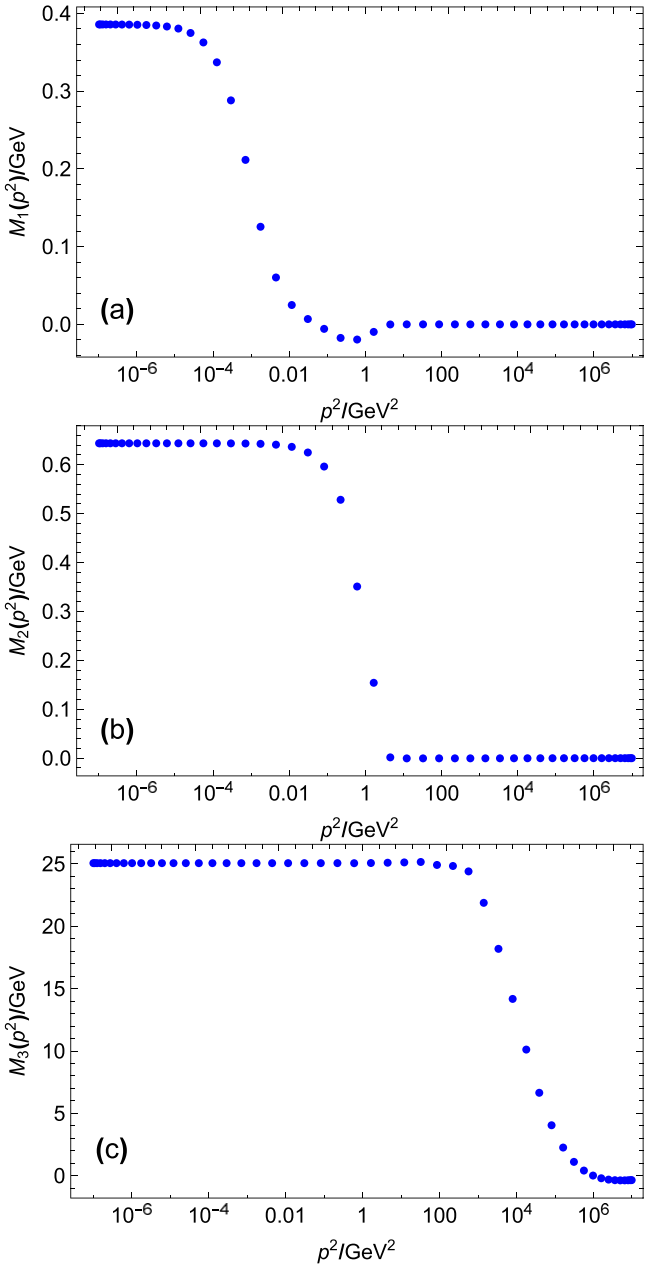

Figure 9. Mass function obtained in terms of p^2. The parameters $e^2 = 21$, $\mu^2 = 1000\ \text{GeV}^2$, $\xi^2 = 10^6\ \text{GeV}^2$, $D = 0.9\ \text{GeV}^2$, $\omega = 0.4\ \text{GeV}$, and $m_{11} = m_{22} = 0\ \text{GeV}$ are taken. (a) Mass function of the lightest quark m_1 (can be used as a reference for m_u). (b) Mass function of the intermediate mass quark m_2 (can be used as a reference for m_c). (c) Mass function of the heaviest quark m_3 (can be used as a reference for m_t).

Table 1. Parameter e^2 dependence of the best-fit constituent mass spectrum. See the footnotes for the definitions of qualities in parentheses. $\xi^2 = 10^6\ \mathrm{GeV}^2$, $\mu^2 = 1000\ \mathrm{GeV}^2$, $D = 0.9\ \mathrm{GeV}^2$, $\omega = 0.4$ GeV, and $m_{11} = m_{22} = 0$ GeV. The dimensional quantities are in units of GeV.

e^2	m_1	m_2	m_3
33	0.48[a]	0.95 (0.77)[b]	166 (137)[b]
20	0.51 (0.00080)[c]	0.63 (0.016)[c]	14 (13)[b]

[a] The current mass was not obtained because of the negative value at 2 GeV; refer to (a) in figure 9.
[b] Mass at the pole.
[c] Mass at 2 GeV.

the three generations of up- and down-type quarks as references and fit their mass spectra by changing G_2. The best-fit results are presented in table 1.

We define the value of the mass function at the zero point as the constituent mass of the quark. The current masses of heavy and light quarks adopt different definitions [24] (see the footnotes in the table). Using the three generations of up-type quarks as a reference, we found the optimal G_2 to be 33, as shown in the second row of table 1, with masses from low to high corresponding to the reference values for the u quark (m_1), c quark (m_2), and t quark (m_3). Using the three generations of down-type quarks as a reference, the optimal G_2 is 20, as shown in the third row of table 1, with masses from low to high corresponding to the reference values for the d quark (m_1), s quark (m_2), and b quark (m_3). The specific values may not correspond very well, but the overall magnitude correspondence and trend behavior are generally correct. That is, we can see significant splitting of the masses of different generations of quarks, with higher-generation quarks having more mass and lower-generation quarks having less mass. The constituent masses of all flavor quarks are greater than their current masses. The constituent masses of heavy flavor quarks are almost the same as their current masses, whereas the constituent masses of light flavor quarks are significantly greater than their current masses.

4. Summary

We investigated the flavor-changing effects in a two-flavor hyperquark system with SU(2) flavor symmetry. Utilizing the extended multiflavor DS equations, we found that the flavor symmetry SU(2) is dynamically broken into SO(2). Because of the residual SO(2) symmetry, the flavor-changing effects can be eliminated and do not manifest in the final physical states. However, they still have some physical consequences. For instance, the quark mass eigenstates become misaligned with the flavor eigenstates. By diagonalizing the mass matrix, the quark states are redefined, and the quark masses are distinctly split. We propose that the new quark mass eigenstates with distinct masses can be interpreted as different generations of quarks. This framework allows us to correspond to the mass spectra of the three generations of quarks.

We started with a simple point interaction model. By analytically solving this model, we obtained the structure of the solutions. We found that there are always three sets of closely related solutions, which can be classified into three interrelated ellipses. These solutions generate three distinct masses that correspond to m_{u}, m_{c}, and m_{t}. A similar approach applies to the down-type quark sector. Subsequently, we studied a more realistic interaction model. Although this model can only be solved numerically, we found that the structures of the solutions obtained before still hold. The masses of the different generations of quarks split distinctly, and the constituent masses are always greater than their current masses. The higher-generation quarks have constituent masses that are almost the same as their current masses, whereas for the lower-generation quarks, the constituent masses are much more significant due to dynamic effects.

Acknowledgments

This study was supported by the National Natural Science Foundation of China under Contract Nos. 11435001 and 11775041, and by the National Science Foundation of China under Grants No. 12175007 and No. 12247107. We gratefully acknowledge helpful discussions with Professors Shou-hua Zhu and Qing-hong Cao.

Appendix

The eight nonlinear integration equations for $\{V_i, S_i, T_i, R_i\}$ are as follows:

$$\begin{aligned}1 &= [Z_2^{11}Z_m^{11}m_{11}S_1(p^2) + Z_2^{11}p^2V_1(p^2)\\ &+Z_m^{12}m_{12}R_2(p^2) + Z_\lambda^{12}\lambda_{12}p^2T_2(p^2)]\\ &+\int\frac{\mathrm{d}^4k}{(2\pi)^4}G(p-k)\{3[S_1(k^2)S_1(p^2)\\ &+R_1(k^2)R_2(p^2)]\\ &+[V_1(k^2)V_1(p^2) + T_1(k^2)T_2(p^2)]\\ &\times\left[2p\cdot k + \frac{(p^2+k^2)p\cdot k - 2p^2k^2}{(p-k)^2}\right]\Bigg\},\end{aligned} \tag{A1}$$

$$\begin{aligned}1 &= [Z_m^{21}m_{21}R_1(p^2) + Z_\lambda^{21}\lambda_{21}p^2T_1(p^2)\\ &+Z_2^{22}Z_m^{22}m_{22}S_2(p^2) + Z_2^{22}p^2V_2(p^2)]\\ &+\int\frac{\mathrm{d}^4k}{(2\pi)^4}G(p-k)\\ &\times\{3[R_2(k^2)R_1(p^2) + S_2(k^2)S_2(p^2)]\\ &+[T_2(k^2)T_1(p^2) + V_2(k^2)V_2(p^2)]\\ &\times\left[2p\cdot k + \frac{(p^2+k^2)p\cdot k - 2p^2k^2}{(p-k)^2}\right]\Bigg\},\end{aligned} \tag{A2}$$

$$0 = [Z_2^{11}Z_m^{11}m_{11}R_1(p^2) + Z_2^{11}p^2T_1(p^2) + Z_m^{12}m_{12}S_2(p^2) + Z_\lambda^{12}\lambda_{12}p^2V_2(p^2)] + \int \frac{\mathrm{d}^4k}{(2\pi)^4}G(p-k) \times \{3[S_1(k^2)R_1(p^2) + R_1(k^2)S_2(p^2)] + [V_1(k^2)T_1(p^2) + T_1(k^2)V_2(p^2)] \times \left[2p\cdot k + \frac{(p^2+k^2)p\cdot k - 2p^2k^2}{(p-k)^2}\right]\right\}, \quad \text{(A3)}$$

$$0 = [Z_m^{21}m_{21}S_1(p^2) + Z_\lambda^{21}\lambda_{21}p^2V_1(p^2) + Z_2^{22}Z_m^{22}m_{22}R_2(p^2) + Z_2^{22}p^2T_2(p^2)] + \int \frac{\mathrm{d}^4k}{(2\pi)^4}G(p-k) \times \{3[R_2(k^2)S_1(p^2) + S_2(k^2)R_2(p^2)] + [T_2(k^2)V_1(p^2) + V_2(k^2)T_2(p^2)] \times \left[2p\cdot k + \frac{(p^2+k^2)p\cdot k - 2p^2k^2}{(p-k)^2}\right]\right\}, \quad \text{(A4)}$$

$$0 = p^2[Z_2^{11}S_1(p^2) - Z_2^{11}Z_m^{11}m_{11}V_1(p^2) + Z_\lambda^{12}\lambda_{12}R_2(p^2) - Z_m^{12}m_{12}T_2(p^2)] + \int \frac{\mathrm{d}^4k}{(2\pi)^4}G(p-k) \times \{-3p^2[S_1(k^2)V_1(p^2) + R_1(k^2)T_2(p^2)] + [V_1(k^2)S_1(p^2) + T_1(k^2)R_2(p^2)] \times \left[2p\cdot k + \frac{(p^2+k^2)p\cdot k - 2p^2k^2}{(p-k)^2}\right]\right\}, \quad \text{(A5)}$$

$$0 = p^2[Z_\lambda^{21}\lambda_{21}R_1(p^2) - Z_m^{21}m_{21}T_1(p^2) + Z_2^{22}S_2(p^2) - Z_2^{22}Z_m^{22}m_{22}V_2(p^2)] + \int \frac{\mathrm{d}^4k}{(2\pi)^4}G(p-k) \times \{-3p^2[R_2(k^2)T_1(p^2) + S_2(k^2)V_2(p^2)] + [T_2(k^2)R_1(p^2) + V_2(k^2)S_2(p^2)] \times \left[2p\cdot k + \frac{(p^2+k^2)p\cdot k - 2p^2k^2}{(p-k)^2}\right]\right\}, \quad \text{(A6)}$$

$$0 = p^2[Z_2^{11}R_1(p^2) - Z_2^{11}Z_m^{11}m_{11}T_1(p^2) + Z_\lambda^{12}\lambda_{12}S_2(p^2) - Z_m^{12}m_{12}V_2(p^2)] + \int \frac{\mathrm{d}^4k}{(2\pi)^4}G(p-k) \times \{-3p^2[S_1(k^2)T_1(p^2) + R_1(k^2)V_2(p^2)] + [V_1(k^2)R_1(p^2) + T_1(k^2)S_2(p^2)] \times \left[2p\cdot k + \frac{(p^2+k^2)p\cdot k - 2p^2k^2}{(p-k)^2}\right]\right\}, \quad \text{(A7)}$$

$$0 = p^2[Z_\lambda^{21}\lambda_{21}S_1(p^2) - Z_m^{21}m_{21}V_1(p^2) + Z_2^{22}R_2(p^2) - Z_2^{22}Z_m^{22}m_{22}T_2(p^2)] + \int \frac{\mathrm{d}^4k}{(2\pi)^4}G(p-k) \times \{-3p^2[R_2(k^2)V_1(p^2) + S_2(k^2)T_2(p^2)] + [T_2(k^2)S_1(p^2) + V_2(k^2)R_2(p^2)] \times \left[2p\cdot k + \frac{(p^2+k^2)p\cdot k - 2p^2k^2}{(p-k)^2}\right]\right\}. \quad \text{(A8)}$$

Using $\{CV_{ij}, CS_{ij}, CT_{ij}, CR_{ij}\}$ $(i = 1,2)$, we obtained the following simplified equations:

$$1 = [Z_2^{11}Z_m^{11}m_{11}S_1(p^2) + Z_2^{11}p^2V_1(p^2) + Z_m^{12}m_{12}R_2(p^2) + Z_\lambda^{12}\lambda_{12}p^2T_2(p^2)] + \frac{3\pi}{2}CS_{11}S_1(p^2) + \frac{3\pi}{2}CR_{11}R_2(p^2) - \frac{3\pi}{4}p^2CV_{11}V_1(p^2) + \frac{\pi}{4}p^4CV_{12}V_1(p^2) - \frac{3\pi}{4}p^2CT_{11}T_2(p^2) + \frac{\pi}{4}p^4CT_{12}T_2(p^2), \quad \text{(A9)}$$

$$1 = [Z_m^{21}m_{21}R_1(p^2) + Z_\lambda^{21}\lambda_{21}p^2T_1(p^2) + Z_2^{22}Z_m^{22}m_{22}S_2(p^2) + Z_2^{22}p^2V_2(p^2)] + \frac{3\pi}{2}CR_{21}R_1(p^2) + \frac{3\pi}{2}CS_{21}S_2(p^2) - \frac{3\pi}{4}p^2CT_{21}T_1(p^2) + \frac{\pi}{4}p^4CT_{22}T_1(p^2) - \frac{3\pi}{4}p^2CV_{21}V_2(p^2) + \frac{\pi}{4}p^4CV_{22}V_2(p^2), \quad \text{(A10)}$$

$$0 = [Z_2^{11}Z_m^{11}m_{11}R_1(p^2) + Z_2^{11}p^2T_1(p^2) + Z_m^{12}m_{12}S_2(p^2) + Z_\lambda^{12}\lambda_{12}p^2V_2(p^2)] + \frac{3\pi}{2}CS_{11}R_1(p^2) + \frac{3\pi}{2}CR_{11}S_2(p^2) - \frac{3\pi}{4}p^2CV_{11}T_1(p^2) + \frac{\pi}{4}p^4CV_{12}T_1(p^2) - \frac{3\pi}{4}p^2CT_{11}V_2(p^2) + \frac{\pi}{4}p^4CT_{12}V_2(p^2), \quad \text{(A11)}$$

$$0 = [Z_m^{21}m_{21}S_1(p^2) + Z_\lambda^{21}\lambda_{21}p^2V_1(p^2) + Z_2^{22}Z_m^{22}m_{22}R_2(p^2) + Z_2^{22}p^2T_2(p^2)] + \frac{3\pi}{2}CR_{21}S_1(p^2) + \frac{3\pi}{2}CS_{21}R_2(p^2) - \frac{3\pi}{4}p^2CT_{21}V_1(p^2) + \frac{\pi}{4}p^4CT_{22}V_1(p^2) - \frac{3\pi}{4}p^2CV_{21}T_2(p^2) + \frac{\pi}{4}p^4CV_{22}T_2(p^2), \quad \text{(A12)}$$

$$0 = [Z_2^{11}S_1(p^2) - Z_2^{11}Z_m^{11}m_{11}V_1(p^2) + Z_\lambda^{12}\lambda_{12}R_2(p^2) - Z_m^{12}m_{12}T_2(p^2)] - \frac{3\pi}{2}CS_{11}V_1(p^2) - \frac{3\pi}{2}CR_{11}T_2(p^2) - \frac{3\pi}{4}CV_{11}S_1(p^2) + \frac{\pi}{4}p^2CV_{12}S_1(p^2) - \frac{3\pi}{4}CT_{11}R_2(p^2) + \frac{\pi}{4}p^2CT_{12}R_2(p^2), \quad \text{(A13)}$$

$$0 = [Z_\lambda^{21}\lambda_{21}R_1(p^2) - Z_m^{21}m_{21}T_1(p^2) + Z_2^{22}S_2(p^2) - Z_2^{22}Z_m^{22}m_{22}V_2(p^2)] - \frac{3\pi}{2}CR_{21}T_1(p^2) - \frac{3\pi}{2}CS_{21}V_2(p^2) - \frac{3\pi}{4}CT_{21}R_1(p^2) + \frac{\pi}{4}p^2CT_{22}R_1(p^2) - \frac{3\pi}{4}CV_{21}S_2(p^2) + \frac{\pi}{4}p^2CV_{22}S_2(p^2), \tag{A14}$$

$$0 = [Z_2^{11}R_1(p^2) - Z_2^{11}Z_m^{11}m_{11}T_1(p^2) + Z_\lambda^{12}\lambda_{12}S_2(p^2) - Z_m^{12}m_{12}V_2(p^2)] - \frac{3\pi}{2}CS_{11}T_1(p^2) - \frac{3\pi}{2}CR_{11}V_2(p^2) - \frac{3\pi}{4}CV_{11}R_1(p^2) + \frac{\pi}{4}p^2CV_{12}R_1(p^2) - \frac{3\pi}{4}CT_{11}S_2(p^2) + \frac{\pi}{4}p^2CT_{12}S_2(p^2), \tag{A15}$$

$$0 = [Z_\lambda^{21}\lambda_{21}S_1(p^2) - Z_m^{21}m_{21}V_1(p^2) + Z_2^{22}R_2(p^2) - Z_2^{22}Z_m^{22}m_{22}T_2(p^2)] - \frac{3\pi}{2}CR_{21}V_1(p^2) - \frac{3\pi}{2}CS_{21}T_2(p^2) - \frac{3\pi}{4}CT_{21}S_1(p^2) + \frac{\pi}{4}p^2CT_{22}S_1(p^2) - \frac{3\pi}{4}CV_{21}R_2(p^2) + \frac{\pi}{4}p^2CV_{22}R_2(p^2). \tag{A16}$$

References

[1] Frampton P H 1996 *Prog. Theor. Phys. Suppl.* **123** 327–35
[2] Maltoni M, Schwetz T, Tórtola M and Valle J W F 2004 Status of global fits to neutrino oscillations *New J. Phys.* **6** 122
[3] Capozzi F, Lisi E, Marrone A, Montanino D and Palazzo A 2016 Neutrino masses and mixings: Status of known and unknown 3ν parameters *Nucl. Phys.* B **908** 218–34
[4] Gonzalez-Garcia M C, Maltoni M, Pena-Garay C and Valle J W F 2001 Global three-neutrino oscillation analysis of neutrino data *Phys. Rev.* D **63** 033005
[5] Aker M *et al* 2022 Direct neutrino-mass measurement with sub-electronvolt sensitivity *Nat. Phys.* **18** 160–6
[6] Panico G and Wulzer A 2016 The composite nambu-goldstone higgs *Lecture Notes in Physics* 913 (Berlin: Springer) 17–75
[7] von Gersdorff G, Ponton E and Rosenfeld R 2015 The Dynamical Composite Higgs *J. High Energy Phys.* **2015** JHEP06(2015)119
[8] Feruglio F, Gavela M B, Kanshin K, Machado P A N, Rigolin S and Saa S 2016 The minimal linear model for the Goldstone Higgs *J. High Energy Phys.* **2016** JHEP06 (2016)038
[9] Cacciapaglia G, Pica C and Sannino F 2020 Fundamental composite dynamics: A review *Phys. Rep.* **877** 1–70
[10] Pomarol A and Tommasini D 1996 Horizontal symmetries for the supersymmetric flavor problem *Nucl. Phys.* B **466** 3–24
[11] Lee C H 2020 Flavor Mixing and Renormalization in a Perturbation Theory 10.48550/arXiv.2011.05330
[12] Espriu D, Manzano J and Talavera P 2002 Flavor mixing, gauge invariance, and wave-function renormalization *Phys. Rev.* D **66** 076002
[13] Aoki K-I, Hioki Z, Kawabe R, Konuma M and Muta T 1983 Electroweak theory *Prog. Theor. Phys. Suppl.* **73** 1–225
[14] Roberts C D and Williams A G 1994 Dyson-schwinger equations and their application to hadronic physics *Prog. Part. Nucl. Phys.* **33** 477–575
[15] Yanagisawa T 2017 Nambu-goldstone bosons characterized by the order parameter in spontaneous symmetry breaking *J. Phys. Soc. Japan* **86** 104711
[16] Hill C T 1990 Dynamical symmetry breaking of the electroweak interactions and the renormalization group *Strong Coupling Gauge Theories and Beyond 25th International Conference on High-energy Physics (ICHEP)* 90 *(Singapore, August 2-8, 1990)* 949–72
[17] King S F and Mannan S H 1990 The top quark condensate *Phys. Lett.* B **241** 249–54
[18] Bardeen W A, Hill C T and Lindner M 1990 Minimal dynamical symmetry breaking of the standard model *Phys. Rev.* D **41** 1647
[19] Suzuki M 1990 Formation of composite higgs bosons from quark-antiquarks at lower energy scales *Mod. Phys. Lett.*A **5** 1205–11
[20] Bai Z, Chang L, Chao J-Y, Gao F and Liu Y-X 2021 Mass dependence of pseudocritical temperature in mean field approximation *Phys. Rev.* D **104** 014005
[21] Blumhofer A and Hutter M 1997 Erratum to "family structure from periodic solutions of an improved gap equation" *Nucl. Phys.* B **494** 485
[22] Maris P and Roberts C D 1997 Differences Between Heavy and Light Quarks arXiv:nucl-th/9710062
[23] Qin S X, Chang L, Liu Y X, Roberts C D and Wilson D J 2011 Interaction model for the gap equation *Phys. Rev.* C **84** 042202
[24] Workman R L 2022 Review of particle physics *PTEP* **2022** 083C01